Experimental analysis and theoretical lift-off criterion for H2/air flames stabilized on a dual swirl injector

Sylvain Marragou, Hervé Magnes, Andrea Aniello, Laurent Selle, Thierry Poinsot, Thierry Schuller

▶ **To cite this version:**

Sylvain Marragou, Hervé Magnes, Andrea Aniello, Laurent Selle, Thierry Poinsot, et al.. Experimental analysis and theoretical lift-off criterion for H2/air flames stabilized on a dual swirl injector. Proceedings of the Combustion Institute, 2023, 39, (4), pp.4345-4354. 10.1016/j.proci.2022.07.255 . hal-03880308

HAL Id: hal-03880308
https://hal.science/hal-03880308

Submitted on 1 Dec 2022

HAL is a multi-disciplinary open access archive for the deposit and dissemination of scientific research documents, whether they are published or not. The documents may come from teaching and research institutions in France or abroad, or from public or private research centers.

L'archive ouverte pluridisciplinaire **HAL**, est destinée au dépôt et à la diffusion de documents scientifiques de niveau recherche, publiés ou non, émanant des établissements d'enseignement et de recherche français ou étrangers, des laboratoires publics ou privés.

Experimental analysis and theoretical lift-off criterion for H_2/air flames stabilized on a dual swirl injector

Sylvain Marragou, Hervé Magnes, Andrea Aniello, Laurent Selle,
Thierry Poinsot and Thierry Schuller

Institut de Mécanique des Fluides de Toulouse, IMFT, Université de Toulouse, CNRS, Toulouse 31400, France

Abstract

Stabilization mechanisms of partially premixed H_2/air flames on a coaxial dual swirl injector are investigated at atmospheric conditions. Hydrogen is injected through a central duct, and the air by the outer annular channel. Both channels are swirled and two stabilization mechanisms are observed depending on the geometrical configuration of the injector and on the operating conditions. In certain regimes, the H_2/air flame stabilizes on the injector lips as a diffusion flame. For other operating conditions, the flame is lifted from the injector and burns in partially premixed regime leading to limited NOx emissions. PIV measurements in cold flow conditions and direct observations of the flame indicate that the flame stabilization mode is mainly controlled by the inner hydrogen swirl level, the injector recess and the hydrogen velocity. For a given air flowrate, a minimum hydrogen velocity to lift the flame is determined for each combination of inner swirl level and injector recess. Assuming the flame close to the injector lips behaves like an edge flame, a model for flame stabilization based on the triple flame speed and the location of the stoichiometric mixture fraction line is built. According to this model, the flame is anchored to the injector if the triple flame can propagate to the inner injector lips, i.e., if the velocity along the stoichiometric line is lower than the triple flame speed. The model is tested using hydrogen diluted with argon and air diluted with nitrogen. Two cases producing predicted opposite trends are verified. First, the stoichiometric line is moved in the direction of lower velocity zone keeping the triple flame speed constant in order to anchor a lifted flame. Next, the stoichiometric line is kept constant and the triple flame speed is reduced in order to lift an anchored flame. The mechanisms driving flame stabilization are discussed.

Keywords: Hydrogen combustion, Swirled burner, Coaxial injector, Stabilization mechanisms, Lifted flames

1. Introduction

Decarbonization of lean combustion processes by burning hydrogen, produced via low-carbon processes such as water electrolysis with renewable electricity [1], raises several issues. Compared to natural gas, hydrogen combustion can result in higher NOx emissions, increased propensity to flashback and higher thermal load on the combustor walls [2, 3].

The high laminar burning velocity of premixed hydrogen air mixtures increases flashback risks limiting the operability range of the burner [4, 5]. This could be avoided by injecting reactants separately inside the combustion chamber, but this strategy generally leads to unacceptable NOx emissions typical of diffusion flames [2, 4]. To promote both low NOx hydrogen combustion and limited flashback risks, new generations of hydrogen injection schemes are developed, as for example technologies based on micromix burners in which miniaturized hydrogen jets are injected into air cross-flows through small air guiding panels [6]. However, these disruptive injection systems require substantial modifications of the combustion chamber architecture that is generally optimized for swirled burners [7].

An alternative solution is investigated in this study with a dual swirl coaxial injector, called HYLON for HYdrogen LOw Nox burner [8, 9]. In this burner, a swirled hydrogen jet exhausting from a central tube is injected in a swirling annular flow. The late injection of hydrogen prevents flashback issues. Preliminary experiments provided as supplemental material reveal that NOx emissions remain limited when the flame is lifted above the burner. Swirling the hydrogen stream is an efficient way to improve mixing with the annular air stream before combustion. Moreover, the aerodynamic stabilization mode also ensures a low thermal stress on the burner.

Swirling the air stream is a well known way to create a Central Recirculation Zone (CRZ) that helps stabilizing flames away from the solid components of the burner [10, 11]. In a study of flame stabilization above coaxial injectors in which both annular air and central fuel channels are swirled, Yuasa [12] observed that swirling the central fuel jet helps to lift methane flames. However, with hydrogen as fuel, the flames remain anchored to the injector rim, even for sonic hydrogen injection conditions. Mixing between two coaxial jets is improved by adding swirl to the central fuel stream and more specifically for light gases as hydrogen [13]. Recently, Degeneve *et al.* [14, 15] showed that swirling the fuel helps lifting the flame from the fuel injector nozzle in a configuration with swirled annular and internal channels flush mounted with the combustion chamber backplane. For non-swirling central fuel jet, it is known that the impulsion ratio $J = \rho_e u_e^2/(\rho_i u_i^2)$ between the external swirled oxidizer and internal fuel streams is the main parameter controlling flame stabilization [16]. When the fuel is swirled, a high value of the impulsion ratio J was found to be a necessary condition to lift CH_4 oxy-

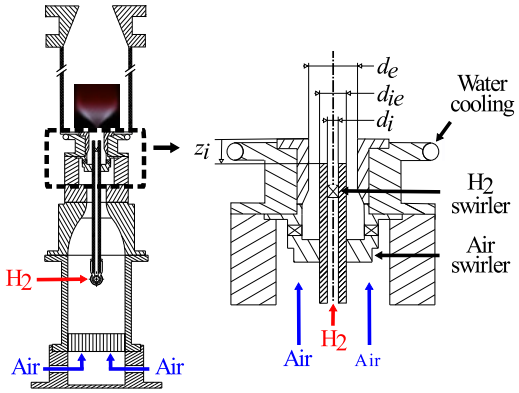

Fig. 1: Experimental setup and main dimensions of the MIRADAS test bench equipped with the HYLON injector.

flames in [14, 15], but the external velocity u_e was not varied in these studies. The detailed physical mechanisms by which the flame anchors or detaches from the burner lips were also not elucidated.

The present study only considers flames powered by pure hydrogen. The objective is to investigate conditions leading to aerodynamically stabilized flames above the HYLON injector. The analysis builds on a set of experiments to unveil the physical mechanisms leading to flame anchoring on the dual swirl burner. The experimental setup and the diagnostics are described in Sec. 2. Analysis of the structure of the cold flow field and of parameters altering flame stabilization are carried out in Sec. 3. These observations are used to extend a stabilization scenario based on a model proposed by Muñiz and Mungal [17] in Sec. 4. Experiments are carried out in Sec. 5 to assess this scenario by triggering flame transitions and compare predictions with the model.

2. Experimental setup

The study is carried out on the MIRADAS test bench [18] shown in Fig. 1 with the HYdrogen LOw NOx (HYLON) dual swirl injector installed on the bench [8]. Inlet flows of hydrogen and air are monitored by two mass flow controllers Brooks SLA 585x series. Air is injected in the plenum, goes through a nozzle and through a radial swirl vane. This vane generates a rotating annular flow with a swirl number S_e = 0.65 in an annular channel of diameter d_e = 18 mm [9]. The hydrogen injector is a tube of internal diameter d_i = 6 mm and external diameter d_{ie} = 10 mm installed inside the annular channel. The recess distance between the outlet sections of the internal hydrogen channel and the external air channel is denoted z_i and can be tuned from z_i = 0 to 8 mm. Different axial swirlers can be installed in the central tube with a swirl number that can be tuned from S_i = 0.0 to 0.9 by modifying the trailing edge angle of the

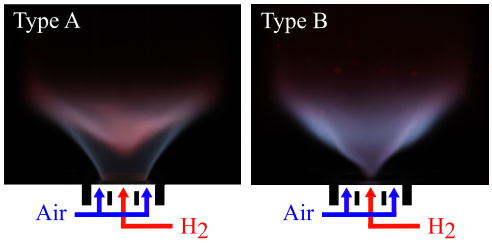

Fig. 2: Hydrogen air flame archetypes stabilized with the HYLON burner. Left: Type A anchored flame. Right: Type B lifted flame.

vane from α_i = 0° to 61° [15]. The swirled flame is confined in a combustion chamber with a square cross section of 78 mm width and 180 mm length. Four quartz windows give optical access to the flow and flame inside the combustion chamber. A nozzle at the outlet of the chamber avoids ambient air recirculation from the surrounding.

Direct flame visualizations are taken with a Nikon D7500 camera equipped with a Nikon AF-S VR Micro-Nikkor 105mm f/2.8G lens. A Particle Image Velocimetry (PIV) system is used to analyze the velocity field in the axial plane of the burner in cold flow conditions. The laser is a double head Quantel Big Sky Laser CFR200. The laser beam passes through a LaVision sheet generator. The height of the laser sheet is approximately 60 mm in the combustion chamber with a 1.5 mm thickness. A SensiCam CCD Imaging 1024×1280 pixels camera equipped with a Nikkor 105mm f/2.8G records the light reflected by micronic mineral oil droplets (Edwards Ultragrade Performance 15) seeded in the flow with a perfume nebulizer. Data acquisition is made with Lavision Davis systems and lasers and the camera are synchronized with a homemade hardware. Data are only presented for the mean velocity fields in this study. They were determined by averages over 1000 instantaneous fields acquired at 4 Hz leading to a statistically converged information.

3. Parametrical analysis of flame lift-off

Two flame archetypes can be stabilized on the HYLON injector as illustrated in the images taken with the Nikon camera in Fig. 2. Type A flame on the left is anchored on the central hydrogen nozzle rim. This flame features two distinct reaction layers. The first one is a bluish inclined reaction layer starting at the injector lips and stabilized in the shear layer between the central hydrogen stream and the external air stream that corresponds to a diffusion flame front. The second one at the top in the center of the CRZ has a reddish color due to H_2O^* chemiluminescence [19] and also corresponds to a diffusion front with hydrogen burning with vitiated air. This stabilization mode is not desired as it results in high NOx emissions (see supplementary material). Moreover, the flame being anchored to the hydrogen injection nozzle, thermal stress drastically reduces the injector lifespan. Temperature measurements of the injector lips with a bichromatic pyrometer indicate that when the flame is lifted above the injector (Type B), the lip temperature remains lower than 250°C and can reach more than 400°C when the flame is anchored to the injector lip (Type A). Tests made in fully premixed injection conditions led to anchored flames with lip temperatures higher than 700°C rapidly leading to flashback. An example of aerodynamically stabilized Type B flame is shown on the right in Fig. 2. This flame has a blue/gray color attributed to the chemiluminescence $H_2O_2^*$ radicals [19, 20]. It is lifted above the HYLON hydrogen injector. This stabilization mode favors mixing of hydrogen and air before combustion with reduced NOx emissions as shown in the supplementary material. It also ensures the injector lifespan.

A parametric study is carried out in the next section to infer the main parameters controlling flame stabilization in the HYLON burner powered by hydrogen.

3.1. Effect of internal swirl level and recess

The HYLON burner in Fig. 1 is flush mounted with the combustion chamber backplane and the recess of the hydrogen channel is first set to zero: $z_i = 0$. PIV data are used to explore conditions leading to a stable and strong CRZ with a co-axial injector when the central fuel injection tube is equipped with a swirler. Figure 3 shows data collected for the same flowrates, without internal swirl $S_i = 0.0$ and with internal swirl $S_i = 0.9$ imparted to the internal hydrogen stream. In these cold flow experiments, hydrogen is replaced by air inside the central tube for safety reason. A choice had to be made to keep either the same momentum or the same Reynolds number of the internal jet when switching from hydrogen to air. It has been preferred to operate the burner with the same bulk flow velocity instead. As discussed in the supplementary material, these conditions lead to the most unfavorable case for the destabilization of the CRZ due to the higher momentum of the central jet when switching from hydrogen to air and keeping the same bulk velocity.

PIV data are only valid 1 mm above the burner outlet in Fig. 3. Without swirl ($S_i = 0.0$), the CRZ produced by the annular swirling flow in Fig. 3a is pushed downstream by the central jet, as already observed in [10, 16]. For this injector geometry, hydrogen flames are always anchored to the central injector rim for all the operating points explored and correspond to type A flames as in Fig. 2a. When the central jet is swirled as in Fig. 3b with $S_i = 0.9$, the size of the CRZ drastically increases and it penetrates inside the central tube leading to a strong flow blockage at the internal injector outlet section between $-0.5 \leq x/d_i \leq 0.5$. This flow blockage is accompanied by large radial velocities close to $x/d_i = \pm 0.5$ [15]. As a consequence, the angle of the swirling jet arms widens. It will be shown that a strong swirl level for the central jet is a necessary but not sufficient condi-

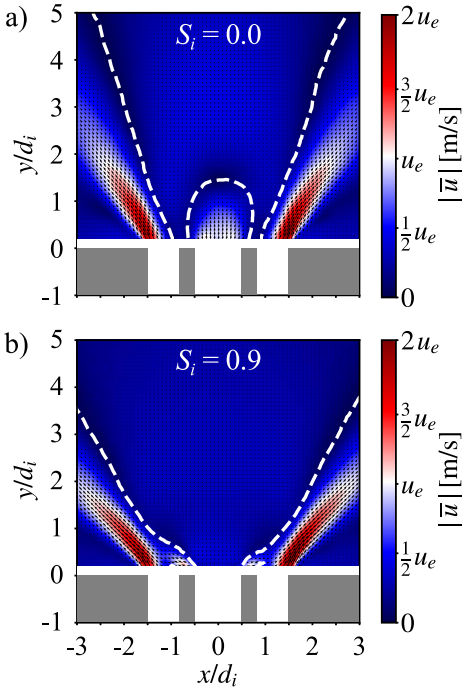

Fig. 3: Mean velocity field in the axial plane for two swirl levels $S_i = 0.0$ (a) and $S_i = 0.9$ (b) and no hydrogen injector recess $z_i = 0$ mm. The fields are normalized by the bulk air velocity $u_e = 29$ m/s in the external channel. The white dashed line denotes the location where the axial velocity $u_z = 0$ m/s, delineating the CRZ.

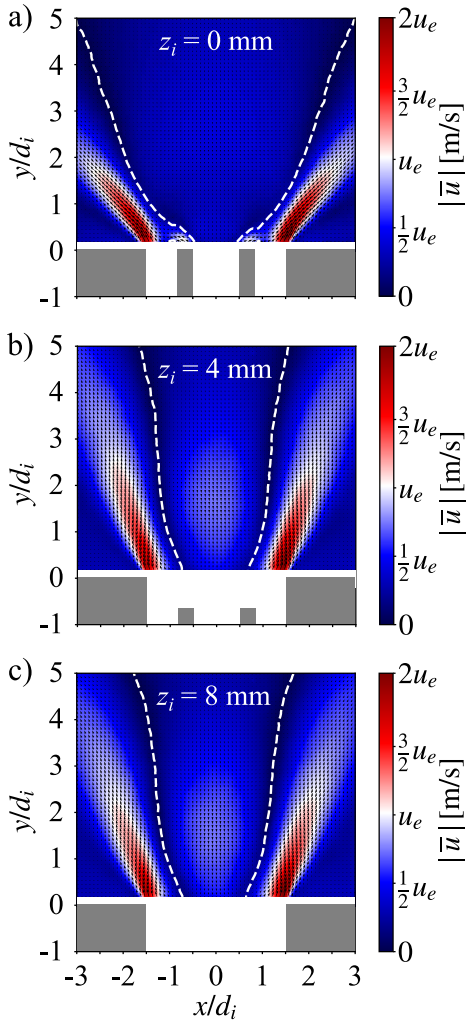

Fig. 4: Mean velocity field in the axial plane when the internal injector recess is varied $z_i = 0$ mm (a) $z_i = 4$ mm (b) and $z_i = 8$ mm (c) for a fixed internal swirl number $S_i = 0.6$. The fields are normalized by the bulk air velocity $u_e = 29$ m/s in the external annular channel. The white dashed line denotes the location where the axial velocity $u_z = 0$ m/s, delineating the CRZ.

tion to lift hydrogen flames and obtain type B flames over a wide range of operating conditions.

These experiments were repeated by keeping constant the internal momentum flux when switching from hydrogen to air. Additional experiments, in hot conditions were also conducted when the annular flow is seeded with zirconium oxide particles. The results are reported as supplementary material. It is shown that the structure of the flow field at the burner outlet is barely altered when the internal jet is swirled between experiments conducted with a constant flowrate and a constant momentum flux of the internal stream. It is also confirmed that the CRZ further expands in the radial direction due to thermal expansion of the burned gases compared to the measurements made under cold flow conditions.

The internal swirl level is now fixed to $S_i = 0.6$ to explore the effect of the recess z_i. Figure 4 shows the structure of the mean velocity field when the recess z_i increases from 0 to 8 mm. The flow field without recess in Fig. 4a is close to that shown in Fig. 3b for a higher swirl level $S_i = 0.9$ but clearly differs from the flow fields shown in Figs. 4b-c when the hydrogen injector outlet section is shifted upstream.

The wide CRZ in Fig. 4a pushes the annular flow radially that features an angle $\alpha = 49^o$ with respect to the burner axis. The recirculation velocity in the CRZ reaches in this case values close to $|u_e|/4$ on the burner axis. For the cases with a recess $z_i = 4$ or 8 mm, the flow field inside the injector is not visible, but Figs. 4b-c clearly show that the swirling jet flow cannot expand as much as in Fig. 4a without recess. The annular jet stream angle reduces to the same value $\alpha = 19^o$ in Figs. 4b and 4c. The two velocity fields in Figs. 4b-c are quite similar despite the different values of the recess z_i of the internal injector. With recess, the CRZ becomes thinner and the highest recirculation velocity increases to values slightly higher than $|u_e|/2$ along the burner axis. This leads to a higher flow blockage of the hydrogen stream with

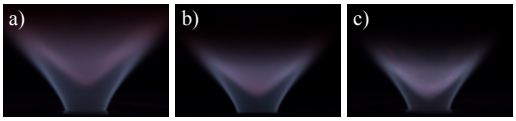

Fig. 5: Impact of the air injection velocity u_e for a fixed hydrogen injection velocity $u_i = 13$ m/s. (a) $u_e = 10$ m/s and $\phi = 0.48$, (b) $u_e = 14$ m/s and $\phi = 0.34$ and (c) $u_e = 22$ m/s and $\phi = 0.22$.

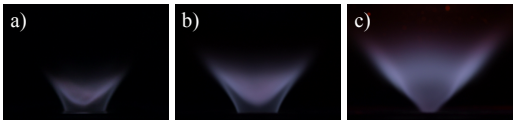

Fig. 6: Impact of the hydrogen injection velocity u_i for a fixed air injection velocity $u_e = 26$ m/s. (a) $u_i = 6$ m/s and $\phi = 0.1$, (b) $u_i = 13$ m/s and $\phi = 0.18$ and (c) $u_i = 32$ m/s and $\phi = 0.46$.

higher radial velocities at the hydrogen nozzle outlet favoring the lifted flame stabilization regime.

In the following experiments, the internal swirl number is set to $S_i = 0.6$ and the injector recess is fixed to $z_i = 4$ mm.

3.2. Effect of air and hydrogen injection velocities

For a given hydrogen flowrate, it is interesting to explore if blowing more air in the external channel can be used to trigger transition from attached to lifted flames. Except blowing at excessively high air flowrates, it was found that increasing the air velocity u_e cannot be used to trigger easily a transition from type A to type B flames. This is illustrated in Fig. 5 for a type A flame anchored on the hydrogen injector. The hydrogen velocity is fixed to $u_i = 13$ m/s and the air velocity is varied from $u_e = 10$ m/s to 22 m/s. The momentum ratio varies in these experiments from $J = 9$ to 41. The flame shortens as u_e increases but remains attached to the hydrogen injector nozzle. This relative insensitivity to the air velocity may originate from a small recirculation region located along the external wall of the hydrogen channel due to the relatively strong swirl $S_e = 0.65$ imparted to the annular air stream. This recirculation causes an aerodynamic flow blockage in the annular air channel and has been identified in companion LES simulations independently of the air flowrate in the annular channel. When looking at transitions between type B to type A flames, it has been found that they slightly depend on the air co-flow velocity.

Effects of the hydrogen injection velocity u_i are now explored by fixing the air flowrate and varying the hydrogen flowrate. The air injection velocity is set to $u_e = 26$ m/s and the hydrogen velocity is increased from $u_i = 6$ to 32 m/s. At low hydrogen injection velocities, the flame belongs to type A anchored on the hydrogen injector in Figs. 6a-b and switches to a type B lifted flame in Fig. 6c for hydrogen injection velocities higher than $u_i = 18$ m/s. A different value is found for a geometrical configuration with a different internal swirl number S_i or injector recess z_i. The threshold value for the hydrogen velocity leading to type B lifted flames also slightly depends on the air velocity. However, for a fixed burner geometry, the hydrogen velocity u_i appears clearly as the main parameter controlling flame stabilization.

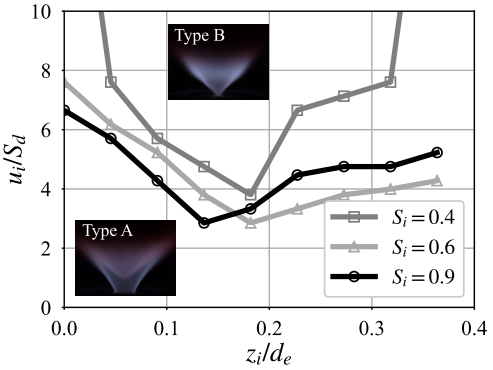

Fig. 7: Type B to type A flame transition as a function of the dimensionless injector recess z_i/d_e and dimensionless hydrogen velocity u_i/S_d for thee values of internal swirl number $S_i = 0.4$, 0.6 and 0.9. External air velocity $u_e = 26$ m/s.

3.3. Stabilization map

For a fixed swirl number $S_e = 0.65$ of the external air stream, the main parameters altering flame stabilization are the internal swirl number S_i, the hydrogen injector recess z_i and the hydrogen injection velocity u_i. Figure 7 plots the hydrogen threshold velocity u_i above which type B lifted flames are observed as a function of the injector recess z_i for different levels of internal swirl S_i. Experiments not shown here indicate that the optimal recess depends on the outer diameter d_e of annular air channel, this is why results are presented as a function of z_i/d_e in Fig. 7. For reasons that will be clarified in section 4, the hydrogen velocity is made dimensionless with the triple flame speed S_d calculated with Eq. (1).

Without internal swirl $S_i = 0.0$, flames remain anchored on the hydrogen injector rim with type A shapes for all tested values of recess and hydrogen injection velocity. For a moderate internal swirl number $S_i = 0.4$, flames are still anchored on the hydrogen injector rim without recess, but can be lifted with recess. For this internal swirl level, the optimal value is obtained for a recess $z_i = 4$ mm. In this case, blowing hydrogen with a velocity higher than $u_i = 24$ m/s leads to lifted flames. This threshold value for the hydrogen velocity above which flames are lifted above the hydrogen injector is designated in the following as the lift-off hydrogen velocity. For a higher in-

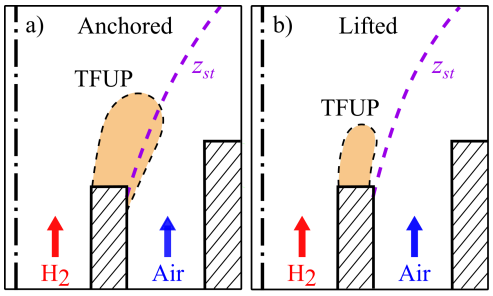

Fig. 8: Schematic representation of the Triple Flame Upstream Propagation TFUP model. a) Case of type A anchored flame. b) Case of type B lifted flame. Within the orange TFUP zone $u < S_d$.

ternal swirl number $S_i = 0.6$, the optimum recess $z_i = 4$ mm remains unaltered, but the lift-off hydrogen velocity drops to $u_i = 18$ m/s. When the internal swirl number is further increased to $S_i = 0.9$, the optimum recess shifts to $z_i = 3$ mm, but the lift-off hydrogen velocity $u_i = 18$ m/s remains unchanged.

These results slightly depend on the air flow velocity which has been set here to $u_e = 26$ m/s.

4. A model for flame re-anchoring

A physical mechanism is now proposed to predict the transition from type B lifted to type A anchored flames. It is clear from the previous results that for a given geometrical configuration of the burner, and more specifically for fixed values of S_e, S_i and z_i, the momentum ratio J is not unequivocally determining the flame stabilization regime.

The issue of lift-off of jet diffusion flames stabilized on a co-axial injector is an old but still active topic in the combustion community [21–23] because it controls blow-off and pollutant emissions from torches. A consensus on the fundamental importance of edge flames was reached in the last 20 years: these edge flames propagate against the flow and allow diffusion flames to find a stabilization point [22]. But it has also become clear that mechanisms leading to flame detachment from a fuel nozzle and re-attachment of a lifted flame to a fuel nozzle may differ and also strongly depend on details of the injector geometry, flow regimes and thermodynamic conditions [23–25]. Except for rocket engines [24], most of these studies are conducted with a small coflow velocity. In the present case, where the flow is recirculating and both the fuel and air streams are swirled, the edge flame concept is used to interpret flame re-attachment as shown now.

Downstream of the hydrogen injector rim in Fig. 8, hydrogen mixes with air with a strong transverse gradient of fuel mass fraction, varying from 1 in the central injector to 0 in the annular external channel. Assuming combustion begins in this region, as for type B flame lifted from the hydrogen injector rim, the leading edge front of the flame corresponds then to an edge flame. An estimation of the maximum displacement velocity of this edge flame can be obtained by considering the limit case of a triple flame. The triple flame speed corresponds to an upper bound of the edge flame speed for a large interval of strain rates except at very low and high strain rates as shown by Cha et al. [26]. A triple flame is an edge flame with a lean, a rich and a stoichiometric branch that propagates towards the injector rim along the stoichiometric mixture fraction line z_{st} [27]. The propagation speed S_d along the z_{st} line of this triple flame can be estimated with [28]:

$$S_d = (\rho_u/\rho_b)^{1/2} S_L \qquad (1)$$

where the laminar burning velocity S_L and the volumetric thermal expansion ratio ρ_u/ρ_b are calculated at stoichiometry.

Following Muñiz and Mungal [17], a triple flame can anchor on the injector only if the triple flame that propagates along the z_{st} line can find flow velocities which are smaller than S_d along this line. In other words, the flame will move upstream as long as the stoichiometric line z_{st} intersects the zone where the flow axial velocity u is lower than the triple flame speed S_d. This zone colored in orange is denoted TFUP zone for Triple Flame Upstream Propagation in Fig. 8. In Fig. 8a, the stoichiometric line intersects the TFUP. The edge flame is able to propagate upstream and anchor on the hydrogen injector rim giving rise to a type A flame. In Fig. 8b, the stoichiometric line z_{st} lies outside the TFUP and the edge flame cannot propagates upstream due to too high flow velocities. As a consequence, the flame remains a type B lifted flame.

Obviously the TFUP criterion combines an information on mixing, which controls the position of the z_{st} line and an information on the structure of the velocity field, which controls the size and shape of the TFUP zone where $u < S_d$. To verify whether the TFUP is indeed the mechanism controlling the transition between lifted and anchored flames, a precise characterization of the TFUP zone would be needed. Unfortunately, this region of the flow is not directly accessible with optical diagnostics when the hydrogen injector features a non-zero recess z_i. Furthermore, without recess, flames are anchored on the hydrogen nozzle rim making this configuration difficult to test transition scenarios. This is why only indirect validations of the Muñiz and Mungal scenario are presented in this work for a configuration of the HYLON burner with recess.

In the following, values for S_L, ρ_b and ρ_u are calculated with Cantera with a kinetic mechanism for hydrogen oxidation that includes 9 species and 21 reactions [29]. For a freely propagating stoichiometric H_2/air premixed flame at ambient condition, one gets $S_L = 2.3$ m/s and $\rho_u/\rho_b = 6.8$, corresponding to a triple flame speed $S_d = 6.1$ m/s deduced from Eq. (1). One also needs to determine the value of the stoichiometric mixture fraction z_{st}. The standard def-

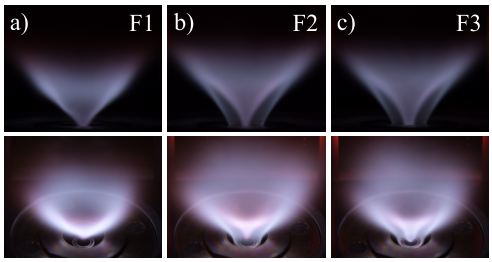

Fig. 9: Type B to type A flame transition triggered by shifting the z_{st} line towards the hydrogen stream while keeping S_d roughly constant for the flames described in Tab. 1. The internal and external injection velocities are fixed here to $u_i = 34$ m/s and $u_e = 28$ m/s. Images are given for two view angles to highlight the flame root.

Table 1: Impact of argon dilution of the hydrogen stream on stoichiometric mixture fraction z_{st} and triple flame speed S_d. Values for S_d are given in m/s.

Flame	ϕ	$Y_{Ar,i}$	$Y_{N2,e}$	z_{st}	S_d
F1	0.46	0.00	0.76	0.028	6.1
F2	0.43	0.51	0.76	0.069	5.9
F3	0.39	0.73	0.76	0.114	5.6

inition is retained, i.e. $z_{st}^{-1} = 1 + 8Y_{H_2,i}/Y_{O_2,e}$, without considering preferential diffusion as it was shown to give good results for H_2/air flames [30]. In this expression, $Y_{H_2,i}$ and $Y_{O_2,e}$ are the hydrogen and oxygen mass fractions injected in the internal and external channels. Since hydrogen and air are injected separately, the stoichiometric line $z_{st} = 0.028$ lies close to the pure air stream.

5. Comparison with experiments

To test the validity of the TFUP zone scenario, one possibility is to push the z_{st} line into or outside the TFUP zone to check if this leads to the expected transition. Here, two sets of experiments were conducted in which the position of the stoichiometric mixture fraction line and the value of the theoretical triple flame speed were modified to trigger a transition from one flame type to the other and test the validity of TFUP zone model.

5.1. Influence of z_{st} line position

First the influence of the position of the z_{st} line with respect to the TFUP zone is explored. For the type B lifted flame shown in Fig. 9a, the z_{st} line should lie outside the TFUP zone according to Fig. 8b. The objective is to trigger a transition to type A flame by shifting the position of the z_{st} line towards the hydrogen injector so that it intersects the TFUP zone as in Fig. 8a without altering the triple flame speed and the aerodynamic flow field, i.e. the boundary of the TFUP zone. To achieve this purpose, the hydrogen stream is diluted with argon. Due to the large difference in molar weight, a small fraction of argon in the hydrogen channel substantially alters the hydrogen mass fraction $Y_{H_2,i}$, but the triple flame speed S_d remains barely modified as indicated in Tab. 1.

In Fig. 9, hydrogen is progressively replaced by argon in the internal injection channel by increasing the argon mass fraction from $Y_{Ar,i} = 0$ to 0.73. This dilution barely changes the triple flame speed S_d, but leads to a large shift of the stoichiometric mixture fraction from $z_{st} = 0.028$ to 0.114 that moves towards the hydrogen stream favoring its intersection with the TFUP zone and consequently also flame reattachment. The injection velocities in the external and internal channels being in these experiments fixed to $u_e = 28$ m/s and $u_i = 34$ m/s, one may assume that the flow field is only weakly perturbed by the fuel dilution and in particular the location of the TFUP zone should not be modified between flames F1 to F3.

The expected transition from type B to type A flame is indeed observed between flames F1 and F2 in Figs. 9a-b. This result is particularly counter-intuitive as for many burners operating at globally lean conditions, fuel dilution generally leads to less well anchored flames. The opposite is observed here in agreement with the TFUP zone model prediction, which constitutes a good indication of the model validity. It is also worth noting that, even if the value of S_d slightly drops from flames F1 to F3 in Tab. 1, this small reduction favors flame detachment while the opposite is observed with flame re-attachment due to the large displacement of the stoichiometric line z_{st} towards the burner centerline.

5.2. Influence of triple flame speed

Now, the stoichiometric mixture fraction remains equal to $z_{st} = 0.028$ as for the pure hydrogen and air streams, but this dilution scheme has a strong impact on the triple flame speed S_d. It is reduced by half from $S_d = 6.1$ m/s for flame F4 in Fig. 10a to $S_d = 3.1$ m/s for flame F6 in Fig. 10c while the position of the stoichiometric line z_{st} inside the flow remains unaltered as indicated in Tab. 2. The air and hydrogen velocities are here set respectively to $u_e = 15$ m/s and $u_i = 14$ m/s. The hydrogen injection velocity being lower than the lift-off hydrogen velocity $u_i = 18$ m/s, a type A anchored flame is observed for flame F4 in Fig. 10a for injection of air and hydrogen.

For this dilution scheme, increasing the fuel and oxidizer dilution rates while keeping the same injection velocities in both channels, the size of the TFUP shrinks as the triple flame speed S_d is reduced from flame F4 to F6 in Tab. 2. The position of the line $z_{st} = 0.028$ inside the flow remaining unaffected, it will not intersect anymore the TFUP zone for a sufficient dilution rate.

This prediction of the TFUP zone model corresponds to what is shown in Fig. 10 between flames F5 and F6. Due to a drop of the flame luminosity with dilution, images have been over-exposed to keep

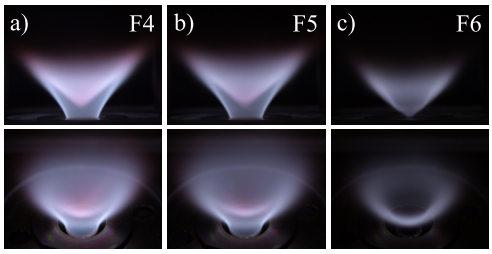

Fig. 10: Type A to type B flame transition triggered by reducing the triple flame speed S_d keeping z_{st} constant for flames described in Tab. 2. The internal and external injection velocities are fixed here to $u_i = 14$ m/s and $u_e = 15$ m/s. Images are given for two view angles to highlight the flame root.

Table 2: Impact of argon dilution of the hydrogen stream and dinitrogen dilution in the air stream on stoichiometric mixture fraction z_{st} and triple flame speed S_d. Values for S_d are given in m/s.

Flame	ϕ	$Y_{Ar,i}$	$Y_{N2,e}$	z_{st}	S_d
F4	0.34	0.00	0.76	0.028	6.1
F5	0.40	0.16	0.79	0.028	4.4
F6	0.46	0.27	0.82	0.028	3.1

the same camera settings for all experiments with dilution. Figures 10a-b show that flames F4 and F5 are well anchored on the hydrogen injector (type A), the last one F6 being lifted away (type B) from the hydrogen injector rim when the triple flame speed drops to $S_d = 3.1$ m/s (Tab. 2).

6. Discussion

The present experiments shed light on the mechanisms leading to flame re-attachment to the hydrogen injector nozzle from the dual swirl coaxial injector. The influence of the internal swirl level of the hydrogen stream in the internal channel can be interpreted as follows. When hydrogen is injected without swirl, a relatively long TFUP zone, characterized by low axial velocities $u \leq S_d$, develops in the wake of the hydrogen injector lips (Fig. 3a). This low velocity region, where hydrogen mixes with air, contains the z_{st} line and hydrogen flames remain anchored for all conditions explored. Adding swirl to the hydrogen stream leads to a flow blockage at the hydrogen injector outlet with a strong radial deflection of the hydrogen stream that has two major effects. The axial extension of the TFUP in the wake of the hydrogen injector shrinks (Fig. 3b) and the z_{st} line is pushed in the direction of the annular flow.

The hydrogen injector recess helps creating larger hydrogen recirculation velocities at the hydrogen injector outlet (Fig. 4). Higher recirculation velocities in the CRZ lead to a stronger flow blockage at the hydrogen injector outlet accompanied by a larger radial deflection of the hydrogen stream towards the air stream. The annular air flow being confined, this also leads to higher air velocities at the hydrogen injector outlet leading to a further reduction of the TFUP size. Moreover, the position of the stoichiometric line z_{st} with respect to the central tube outlet is also shifted influencing flame stabilization.

The weak impact of air velocity in the annular channel is difficult to interpret with the measurements presented in this work and requires a more detailed analysis of the velocity field inside the HYLON burner. Companion LES simulations are currently exploring this behavior. A small recirculation region along the external wall of the hydrogen injector has been identified as the cause of an aerodynamic flow blockage that seems to be present independently of the air flowrate blowing through the annular channel. These preliminary simulations need however to be confirmed.

7. Conclusion

For a fixed external swirl level of the air stream, the main parameters controlling flame anchoring above a dual swirl H_2/air injector have been identified as the internal swirl level, the recess between the hydrogen and air injectors and the hydrogen injection velocity. Conditions leading to flame lift-off have been shown to comply with a model called TFUP for Triple Flame Upstream Propagation zone, inspired from the pioneering model of Muñiz and Mungal [17].

In particular, it has been shown that:

- swirling the internal hydrogen channel is a necessary but not sufficient condition to lift hydrogen/air flames
- a small recess of the hydrogen nozzle outlet with respect to the annular air injector outlet largely extends the operability domain with lifted flames, the optimum value depending on the inner swirl level
- for the injector geometries explored, the hydrogen injection velocity mainly controls flame stabilization while air velocity has only a minor impact on the observed flame shape transitions
- the physical parameters controlling lifted flame re-attachment to the hydrogen nozzle are the position of the stoichiometric mixture fraction line z_{st} and the triple flame speed S_d
- flames are lifted when the stoichiometric z_{st} line lies outside a TFUP zone, defined as the region where the axial flow velocity is lower than the triple flame speed S_d

These results help to understand flame stabilization above injectors powered by hydrogen, a critical issue for the new generation of gas turbines.

8. Supplementary material

NOx measurements and additional PIV measurements in cold and hot flow conditions are provided as supplementary material.

9. Acknowledgements

This project has received funding from the European Research Council under the European Union's Horizon 2020 research and innovation program Grant Agreement 832248, SCIROCCO and under the Horizon 2020, COEC (Center of Excellence in Combustion) program, Grant Agreement 952181. The authors are grateful to the technical support from G. Albert, S. Cazin, S. Lun Kwong Leon, M. Marchal, L. Mouneix and R. Soeparno from IMFT.

References

[1] G. Kakoulaki, I. Kougias, N. Taylor, F. Dolci, J. Moya, A. Jäger-Waldau, Green hydrogen in Europe – A regional assessment: Substituting existing production with electrolysis powered by renewables, Energ. Convers. Manage. 228 (2021) 113649.

[2] P. Chiesa, G. Lozza, L. Mazzocchi, Using Hydrogen as Gas Turbine Fuel , J. Eng. Gas Turb. Power 127 (1) (2005) 73–80.

[3] G. Richards, M. McMillian, R. Gemmen, W. Rogers, S. Cully, Issues for low-emission, fuel-flexible power systems, Prog. Energ. Combust. Sci. 27 (2) (2001) 141–169.

[4] O. Tuncer, S. Acharya, J. Uhm, Dynamics, NOx and flashback characteristics of confined premixed hydrogen-enriched methane flames, Int. J. Hydrogen Energ. 34 (1) (2009) 496–506.

[5] C. Eichler, G. Baumgartner, T. Sattelmayer, Experimental Investigation of Turbulent Boundary Layer Flashback Limits for Premixed Hydrogen-Air Flames Confined in Ducts, J. Eng. Gas Turb. Power 134 (1) (11 2011).

[6] H. H.-W. Funke, N. Beckmann, J. Keinz, A. Horikawa, 30 Years of Dry-Low-NOx Micromix Combustor Research for Hydrogen-Rich Fuels—An Overview of Past and Present Activities, J. Eng. Gas Turb. Power 143 (7) (03 2021).

[7] S. Boerner, H. H. W. Funke, P. Hendrick, E. Recker, R. Elsing, Development and integration of a scalable low NOx combustion chamber for a hydrogen-fueled aerogas turbine, EUCASS P. Series 4 (2013) 357–372.

[8] S. Richard, C. Viguier, S. Marragou, T. Schuller, Dispositif d'injection de dihydrogène et d'air (FR Patent No FR2111267), Institut National de la Propriété Industrielle, 2021.

[9] S. Marragou, H. Magnes, T. Poinsot, L. Selle, T. Schuller, Stabilization regimes and pollutant emissions from a dual fuel CH4/H2 and dual swirl low NOx burner, Int. J. Hydrogen Energ. 47 (44) (2022) 19275–19288.

[10] T. F. Dixon, J. S. Truelove, T. F. Wall, Aerodynamic Studies on Swirled Coaxial Jets From Nozzles With Divergent Quarls, J. Fluid. Eng. 105 (2) (1983) 197–203.

[11] M. D. Durbin, M. D. Vangsness, D. R. Ballal, V. R. Katta, Study of Flame Stability in a Step Swirl Combustor, J. Eng. Gas Turb. Power 118 (2) (1996) 308–315.

[12] S. Yuasa, Effects of swirl on the stability of jet diffusion flames, Combust. Flame 66 (2) (1986) 181–192.

[13] S. Chouaieb, W. Kriaa, H. Mhiri, P. Bournot, Swirl generator effect on a confined coaxial jet characteristics, Int. J. Hydrogen Energ. 42 (48) (2017) 29014–29025.

[14] A. Degeneve, C. Mirat, J. Caudal, R. Vicquelin, T. Schuller, Effects of Swirl on the Stabilization of Non-Premixed Oxygen-Enriched Flames Above Coaxial Injectors, J. Eng. Gas Turb. Power 141 (121018 (9 pages)) (2019).

[15] A. Degeneve, R. Vicquelin, C. Mirat, J. Caudal, T. Schuller, Impact of co- and counter-swirl on flow recirculation and liftoff of non-premixed oxy-flames above coaxial injectors, Proc. Combust. Inst. 38 (4) (2021) 5501–5508.

[16] R.-H. Chen, J. F. Driscoll, J. Kelly, M. Namazian, R. W. Schefer, A Comparison of Bluff-Body and Swirl-Stabilized Flames, Combust. Sci. Technol. 71 (4-6) (1990) 197–217.

[17] L. Muñiz, M. Mungal, Instantaneous flame-stabilization velocities in lifted-jet diffusion flames, Combust. Flame 111 (1) (1997) 16–31.

[18] G. Oztarlik, L. Selle, T. Poinsot, T. Schuller, Suppression of instabilities of swirled premixed flames with minimal secondary hydrogen injection, Combust. Flame 214 (2020) 266–276.

[19] R. W. Schefer, W. D. Kulatilaka, B. D. Patterson, T. B. Settersten, Visible emission of hydrogen flames, Combust. Flame 156 (6) (2009) 1234–1241.

[20] T. Fiala, T. Sattelmayer, Heat release and UV–Vis radiation in non-premixed hydrogen–oxygen flames, Exp. Fluids 56 (2015) 1–15.

[21] R. Schefer, M. Namazian, J. Kelly, Stabilization of lifted turbulent-jet flames, Combust. Flame 99 (1) (1994) 75–86.

[22] A. Upatnieks, J. Driscoll, C. Rasmussen, S. Ceccio, Liftoff of turbulent jet flames—assessment of edge flame and other concepts using cinema-piv, Combust. Flame 138 (2004) 259–272.

[23] T. F. Guiberti, W. R. Boyette, A. R. Masri, W. L. Roberts, Detachment mechanisms of turbulent non-premixed jet flames at atmospheric and elevated pressures, Combust. Flame 202 (2019) 219–227.

[24] G. Singla, P. Scouflaire, J. Rolon, S. Candel, Flame stabilization in high pressure lox/gh2 and gch4 combustion, Proc. Combust. Inst. 31 (2007) 2215–2222.

[25] T. Guiberti, W. Boyette, W. Roberts, A. Masri, Pressure effects and transition in the stabilization mechanism of turbulent lifted flames, Proc. Combust. Inst. 37 (2) (2019) 2167–2174.

[26] M. S. Cha, P. D. Ronney, Propagation rates of non-premixed edge flames, Combust. Flame 146 (1) (2006) 312–328.

[27] H. Im, J. Chen, Structure and propagation of triple flames in partially premixed hydrogen–air mixtures, Combust. Flame 119 (4) (1999) 436–454.

[28] G. R. Ruetsch, L. Vervisch, A. Liñán, Effects of heat release on triple flames, Phys. Fluids 7 (6) (1995) 1447–1454.

[29] R. Mével, S. Javoy, F. Lafosse, N. Chaumeix, G. Dupré, C.-E. Paillard, Hydrogen–nitrous oxide delay times: Shock tube experimental study and kinetic modelling, P. Combust. Inst. 32 (1) (2009) 359–366.

[30] R. S. Barlow, M. J. Dunn, G. Magnotti, Preferential transport effects in premixed bluff-body stabilized CH4/H2 flames, Combust. Flame 162 (3) (2015) 727–735.

Supplementary material: NOx measurements and additional PIV data [1]

1 NOx emissions

Pollutant emissions are measured with an ECOM J2KN Pro flue gas analyzer featuring a $\pm$ 1 ppm confidence internal on CO, NO and NO2 concentrations in the dried sampled flue gases. All measurements are normalized by a volumetric fraction of 15% of O2 in the flue gases. The pollutant measurements shown in Fig. 1 are carried out for three fixed values of the equivalence ratio $\phi = 0.40$, 0.55 and 0.70 varying the thermal power P delivered by hydrogen. The flame archetype is indicated by the style of the marker: filled markers denote anchored flames (type A) and empty markers correspond to lifted flames (type B) [1]. As expected, NOx emissions increase with the equivalence ratio for both flame archetypes. Flames anchored to the hydrogen injector lips (type A) produce higher NOx levels due to the diffusion structure of the flame reaction layers. Lower NOx levels are observed for lifted type B flames which burn in partially premixed mode. Moreover, NOx emissions drop for all the equivalence ratios considered when the thermal power increases. This intriguing behavior is left for further studies.

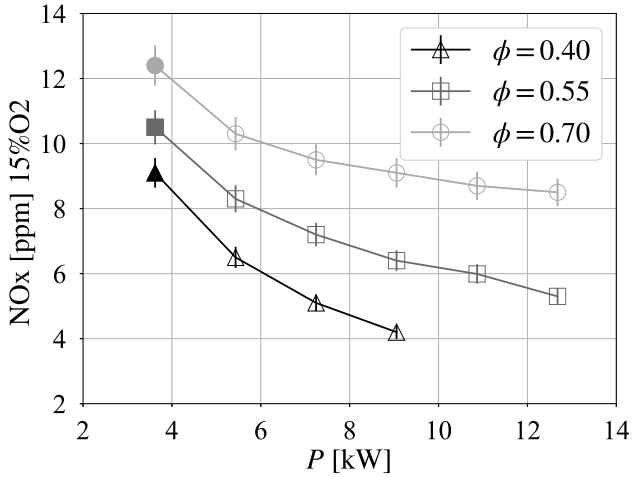

Fig. 1: Impact of thermal power P on NOx emission levels for different equivalence ratios $\phi = 0.4$, 0.55 and 0.70. Filled markers denote type A anchored flames and empty markers denote type B lifted flames [1].

2 PIV measurements

PIV measurements shown in [1] in cold flow conditions were carried out by replacing the central flow of hydrogen by the same volumetric flowrate of air. This strategy enabled to get a good quality of the

seeding for particles injected through the central tube. But the momentum of the central jet increases in that case with respect to hydrogen injection due to its lower density. Tests were made to explore the impact of this choice on the structure of the flow at the burner outlet.

Figure 2 shows an example of comparison of the flow field in the axial plane for a swirl level $S_i = 0.6$, a recess $z_i = 4$ mm and an air velocity $u_e = 29$ m/s. Figure 2.a shows the case where the bulk velocity $u_i = 34$ m/s in the central tube is equal to the reference operating point in reactive conditions. Figure 2.b shows the case where the momentum ratio $J = 10$ is kept constant between the two streams. The structure of the flow field is similar in both cases. The intensity of the recirculation in the CRZ and the swirling jet spread angle are slightly higher in Fig. 2.a. These differences are however small.

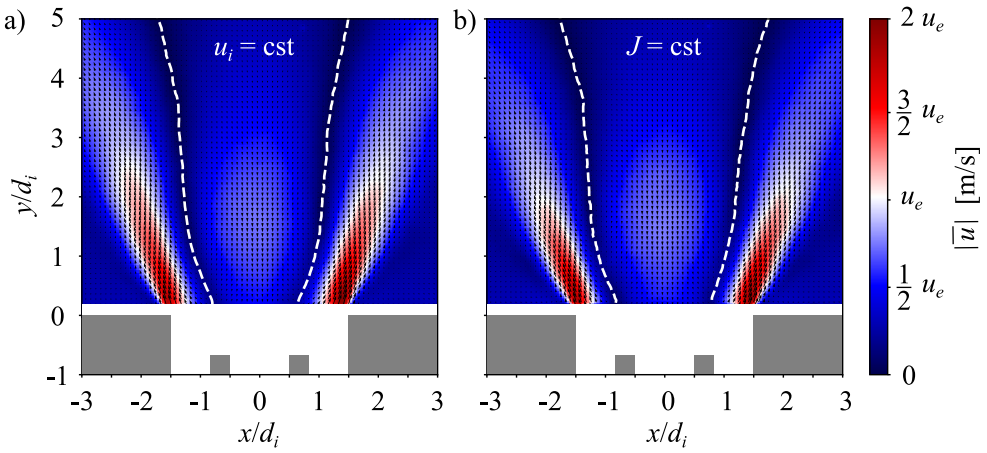

Fig. 2: Isothermal case: Mean velocity field in the axial plane for an internal swirl level $S_i = 0.6$ and a hydrogen injector recess $z_i = 4$ mm with (a) $u_i = 34$ m/s conserved (b) $J = 10$. Results are normalized by the bulk air velocity $u_e = 29$ m/s in the external channel. The white dashed line denotes the location where the axial velocity $u_z = 0$ m/s, delineating the CRZ.

Additional PIV measurements were attempted in reactive conditions. Seeding is achieved with micrometric zirconium oxide particules. Only the air annular channel could be seeded in this case. Results for $u_i = 34$ m/s in Fig. 2 obtained with air in the center should be compared to Fig. 3 obtained for hydrogen injected at the same velocity. The particule density in the hot CRZ is too low to get a statistically meaningful information on the velocity field in this region, but the size of the CRZ can be determined without ambiguity. This figure shows that the deviation angle of the swirling jet is larger than in cold conditions due to the thermal expansion of the burned gases. The CRZ is well developed and stable due to the central swirled injection.

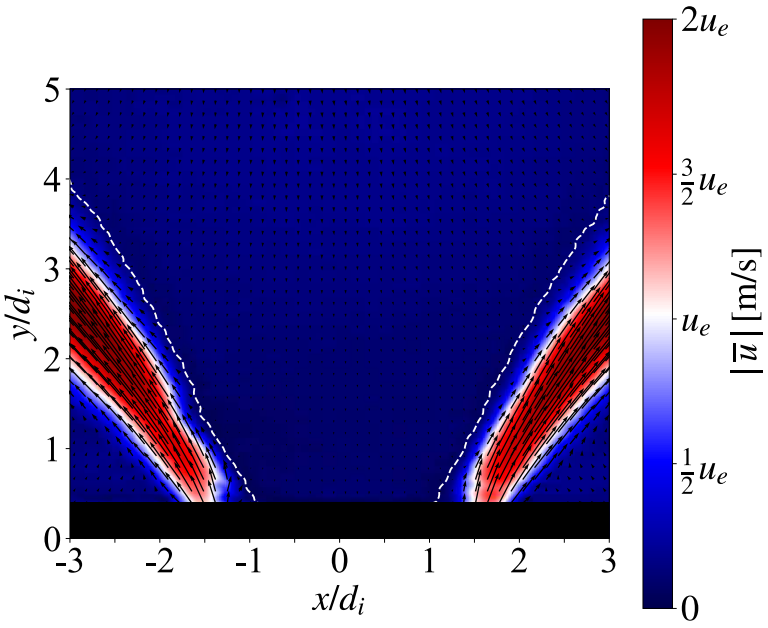

Fig. 3: Reactive case: Mean velocity field in the axial plane for an internal swirl level $S_i = 0.6$ and a hydrogen injector recess $z_i = 4$ mm. Results are normalized by the bulk air velocity $u_e = 29$ m/s in the external channel. The white dashed line denotes the location where the axial velocity $u_z = 0$ m/s, delineating the CRZ.

References

[1] S. Marragou, H. Magnes, A. Aniello, L. Selle, T. Poinsot, T. Schuller, Experimental analysis and theoretical lift-off criterion for h2/air flames stabilized on a dual swirl injector, P. Combust. Inst. 39 (2022) 8 pages.